AGU PUBLICATIONS

Geophysical Research Letters

RESEARCH LETTER
10.1002/2014GL062662

Key Points:
- Site amplifications between 0.67 to 2 Hz from ambient noise cross correlation
- High-resolution study in Long Beach, CA from 5200 geophone arrays
- New approach uses amplitudes of ambient noise without dependence on sources

Correspondence to:
D. C. Bowden,
dbowden@caltech.edu

Citation:
Bowden, D. C., V. C. Tsai, and F. C. Lin (2015), Site amplification, attenuation, and scattering from noise correlation amplitudes across a dense array in Long Beach, CA, *Geophys. Res. Lett.*, *42*, 1360–1367, doi:10.1002/2014GL062662.

Received 2 DEC 2014
Accepted 27 JAN 2015
Accepted article online 2 FEB 2015
Published online 6 MAR 2015

Site amplification, attenuation, and scattering from noise correlation amplitudes across a dense array in Long Beach, CA

D. C. Bowden[1], V. C. Tsai[1], and F. C. Lin[2]

[1]Seismological Laboratory, Division of Geological and Planetary Sciences, California Institute of Technology, Pasadena, California, USA, [2]Department of Geology and Geophysics, University of Utah, Salt Lake City, Utah, USA

Abstract For accurate seismic hazard evaluation, both the spatial and frequency-dependent variabilities in the amplitudes of earthquake ground motions are needed. While this information is rarely fully available due to the paucity of relevant seismic data, dense arrays like the 5200-geophone array in Long Beach, California provide the opportunity to study this amplitude variability. Here we show that ambient noise correlation amplitudes from the Long Beach array can be used to directly determine frequency-dependent site amplification factors. We analyze Rayleigh-wavefield amplitude gradients from ambient noise correlations that are processed so that relative amplitudes satisfy the wave equation and are therefore meaningful. Ultimately, we construct maps of site amplification across Long Beach at frequencies of 0.67, 1.0, and 2.0 Hz. These maps correlate well with local structure, notably the Newport-Inglewood Fault and also to known velocity structure. Through this process, we also obtain constraints on average attenuation structure and local scattering.

1. Introduction

Traditional seismic hazard studies have primarily focused on describing the expected shaking from potential future earthquakes based on empirical observations of previous earthquakes [e.g., *Abrahamson and Shedlock*, 1997; *Cua and Heaton*, 2012]. These observations have shown that the amplitudes of seismic waves can be strongly affected by shallow crustal heterogeneities. For example, ground motions in sedimentary basins have historically shown significantly higher amplitudes of ground motion compared to hard-rock sites a few kilometers away. Despite attempts to spatially map these variations, the sparsity of available data from historic events usually necessitates reliance on averaged characterizations for a given region or material type (i.e., sediments versus hard rock). Unfortunately, such averages do not describe the complex and frequency-dependent patterns of wave propagation and so often fail to provide realistic estimates of the lateral variability of ground motion amplitudes [*Graves et al.*, 2010].

Effects of shallow crustal heterogeneities on ground motion amplitudes can be observed more robustly and systematically with arrays of seismometers that are dense relative to the features of interest, which have only recently become technologically feasible or affordable. For example, *Lin et al.* [2012] was able to track the Rayleigh wavefronts of distant earthquakes across the USArray to infer site amplification and attenuation, which showed strong agreement with known geologic structure. However, the observations were only available in the lower frequency range of 0.01 to 0.04 Hz (with higher frequencies being too highly attenuated), while engineers studying seismic hazard are often most concerned with building resonances at higher frequencies (i.e., in the range of 0.5–2.0 Hz) [*Kohler et al.*, 2005].

Ambient noise cross correlations provide a signal rich in these higher frequencies and offer the flexibility of making observations in the absence of earthquakes [*Shapiro*, 2004]. A particularly dense array of more than 5200 geophones in Long Beach, CA, with an average station spacing of only 100 m, allowed *Lin et al.* [2013] to track phase traveltimes across the array, and the shallow velocity structure resolved shows strong correlations with the Newport-Inglewood Fault running through the array. Other studies have focused on directly observing amplitudes from ambient noise cross-correlation functions [e.g., *Prieto and Beroza*, 2008; *Denolle et al.*, 2014; *Lin et al.*, 2011; *Zhang and Yang*, 2013], and such methods show promising similarity to observed earthquake amplifications. Careful treatment is required, however, as a heterogeneous

distribution of noise sources can bias the noise correlation amplitudes if not properly accounted for [*Weaver*, 2011; *Tsai*, 2011]. In this paper, we use ambient noise cross correlations of the Long Beach array with the Helmholtz wavefront tracking approach of *Lin et al.* [2012] to recover the spatial variability of site amplifications and demonstrate that tracking amplitudes across an array is insensitive to the initial distribution of those amplitudes. We compare our site amplification results with the phase velocity observations of *Lin et al.* [2013] as well as earthquake and nuclear testing observations.

2. Theoretical Background

The wavefront tracking approach of *Lin et al.* [2012] considers the observed amplitudes $A(x, y)$ and traveltimes $\tau(x, y)$ of a 2-D Rayleigh wavefield (the spatial wavefield corresponding to the Rayleigh wave arrival) across an array and uses the following relation derived from the 2-D Helmholtz wave equation:

$$\frac{2\nabla\beta \cdot \nabla\tau}{\beta} - \frac{2\alpha}{c} + S = \frac{2\nabla A \cdot \nabla\tau}{A} + \nabla^2\tau \tag{1}$$

where β is a local site amplification factor for Rayleigh waves, α is an attenuation constant, and c is phase velocity [*Lin et al.*, 2012]. The term α refers to intrinsic attenuation and relates to the more commonly used Q factor by $\alpha = \pi f/CQ$ where f is frequency and C is group velocity. Here we consider the more general solution of the inhomogeneous Helmholtz equation where a source term, S, (which is explained later) is added to the result of *Lin et al.* [2012]. Based on equation (1), the observed amplitude variation corrected by wavefront focusing and defocusing (i.e., by the $\nabla^2\tau$ term) can be related to the local amplification variation, attenuation, and internal sources (terms on the left-hand side of equation (1)). These terms can be further decoupled, as the effect of both attenuation and internal sources is to consistently and statically decrease or increase amplitudes, respectively, while the site amplification term (quantified by the scalar β) will show different effects depending on the direction of wave propagation (i.e., propagation into or out of a sedimentary basin) [*Lin et al.*, 2012]. The advantage of the wavefront tracking method can be seen in that we are concerned with only local wavefield variations and not the initial conditions of the wave excitation.

To use the wavefront tracking approach on ambient noise cross correlations, we must be able to construct a 2-D wavefield that satisfies the wave equation. Since cross correlation is a linear operator that acts on the background noise wavefield regardless of where that source originates, observations from noise cross correlation between one center station (the virtual source) and all other stations across the array still satisfies the wave equation [*Lin et al.*, 2013]. We can observe both an incoming wavefield from the negative lag times of the cross correlations and an outgoing wavefield from the positive lag times. Importantly, we do not force a symmetric form of the noise correlation function (NCF) in our analysis, as is often done in other noise processing applications [i.e., *Lin et al.*, 2013], because this effectively reverses time for the inward traveling signals and consequently reverses the effect of intrinsic attenuation.

Analyzing the two components separately allows us to determine the effects and strengths of internal, local sources as compared to attenuation. These sources may be any repeated, impulsive source of energy such as highway or factory noise. Similarly, elastic scatterers may be viewed as point sources of energy and, in very geologically heterogeneous regions, this scattering may be the dominant contribution. In either case, when a local source is present, the positive or negative lag cross-correlated signal will increase when the local source is within the corresponding stationary-phase hyperbola of a given station pair [*Snieder*, 2004]. Thus, the incoming noise cross-correlation wavefield (negative lag) will increase in amplitude when passing through the source location, as the focus of the stationary-phase hyperbola is moving with the wavefield. On the other hand, the focus of the stationary-phase hyperbola is fixed at the center station location for the outgoing wavefield (positive lag), and hence, the wavefield amplitude is not going to be affected by the source. Thus, by studying both directionally-dependent incoming and outgoing amplitude variations, the spatial variability of all three terms can, in theory, be resolved.

3. Data and Methods

In order to make use of ambient noise correlation amplitudes from the Long Beach array (or any array), special care must be taken to preserve relative amplitudes and ensure the cross correlations satisfy the wave

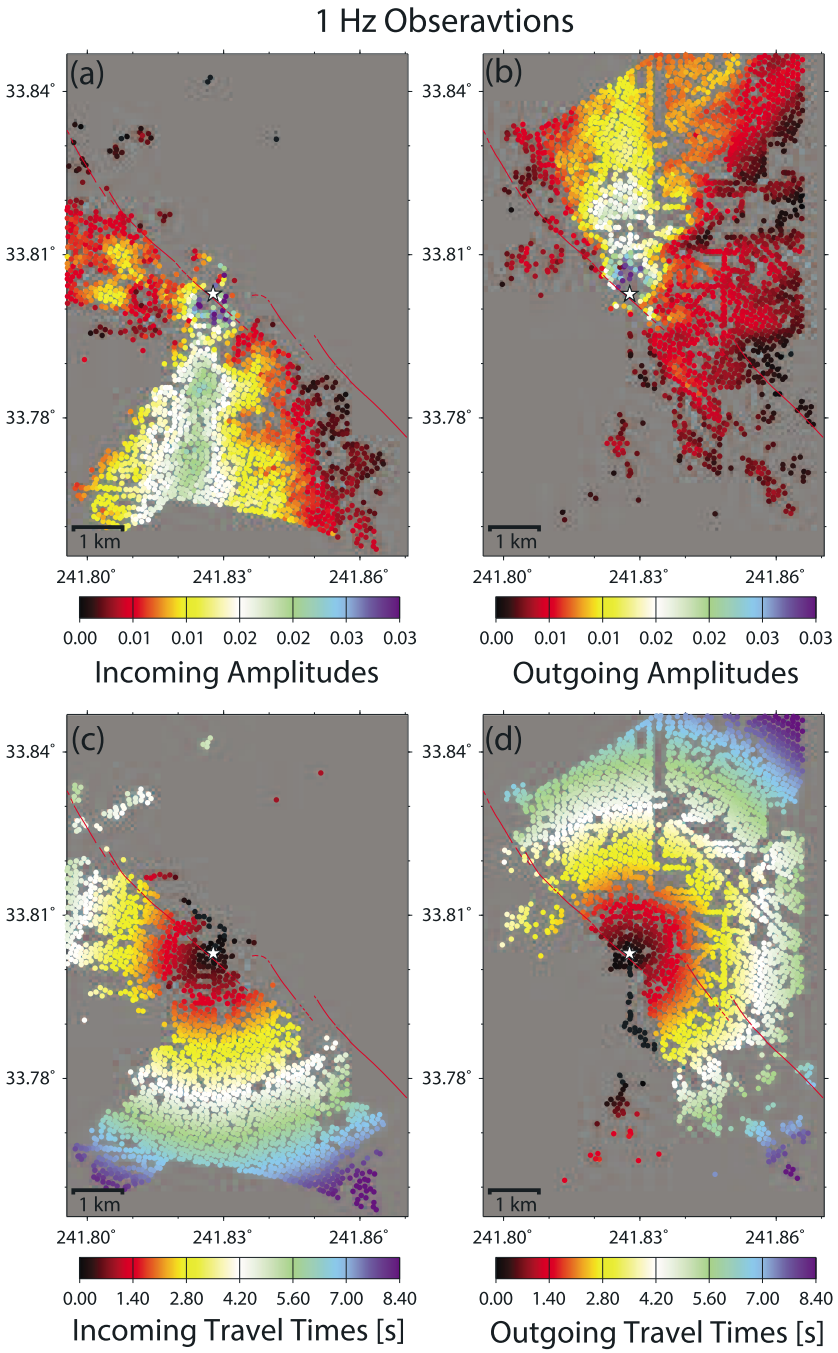

Figure 1. Example observations from NCFs at 1 Hz. Maps of (a) amplitude, *A*, and (c) phase traveltime, τ, of the incoming wavefronts, and maps of (b) amplitude, *A*, and (d) phase traveltime, τ, of the outgoing wavefronts. We observe a strong south-to-north trend in the amplitudes, as signal energy is strongest from near the coastline to the south (with low SNR measurments removed). Note that the amplitudes are treated such that the relative magnitudes are preserved but are normalized and effectively unitless.

equation. One way to ensure this is to use raw waveforms in the cross correlation [*Prieto and Beroza*, 2008], but the noisy urban environment and short time span of our data (about 3 weeks) resulted in raw NCFs for which clear group arrivals could not be determined. Unfortunately, many of the commonly accepted signal processing techniques such as time domain normalization or spectral prewhitening [*Bensen et al.*, 2007] act on a signal by smoothing, normalizing, or otherwise altering that specific signal. Such individual

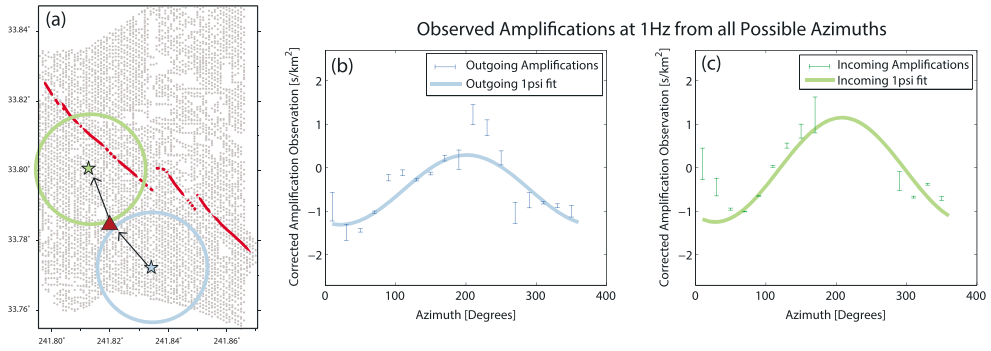

Figure 2. (a) Example of how observed amplifications (both outgoing in blue and incoming in green) provide multiple directions of measurement for a given point, shown with a red triangle. These observations and corresponding 1ψ fits for (b) outgoing and (c) incoming waves treated independently. Error bars represent 1 sigma confidence intervals and are omitted where no observations were present. Differences in the vertical offsets of the 1ψ fits can be explained by the fact that sources are only seen on the incoming wavefronts, while the difference in magnitude may result from numerical uncertainties.

modifications to a waveform nonlinearly affect the relative signal amplitudes and our assumptions about the wave equation would no longer hold. To maintain linearity, any processing must be applied equally across all signals for the same time period. To accomplish this, we whiten all of the spectra for a given hour using a single spectral envelope that represents the 95th percentile of the entire 5200-station array. Similarly, once the noise cross correlations have been computed for a given hour, we consider the 95th percentile of all NCF peak amplitudes for the hour and inversely weight each record by this number before including them in the final stack. These whole-array techniques are not as effective at cleaning up the group arrivals as single station treatments, but they do accomplish the same goal of increasing the NCF's signal-to-noise ratio by reducing the effect of noise sources that are impulsive in time, space, or frequency [*Weaver*, 2010], while maintaining linearity.

Using all possible stations as virtual sources, maps describing phase traveltimes, τ, and the associated amplitudes, A, were collected at narrow band-pass windows of 0.67 Hz, 1.0 Hz, and 2.0 Hz (e.g., as in Figure 1). Measurements are only selected for which the signal-to-noise ratio (SNR, defined as peak amplitude divided by the root-mean-square of the trace) is above a cutoff: SNR $>$ 8 at 0.67 Hz and 1 Hz, and SNR $>$ 4 at 2 Hz. We note that while an identical selection criterion of SNR $>$ 4 can be used for the three frequencies, pushing this threshold higher where possible allows us to suppress spurious measurements and reduce overall uncertainties. The actual results are minimally affected by SNR since our method is theoretically not affected by correlation noise level, unlike with coherency methods. A strong northward "cone" of energy is apparent in the amplitude maps for both the inward and outward propagation directions and is associated with a stronger source of noise energy from the coastline along the southern border of the array. Weak directions are also apparent, including large areas for which the data have been suppressed by the SNR cutoff. Although urban sources of noise should be strong in the region, northward traveling energy dominates the raw waveforms at these frequencies and so the cross correlations are sensitive predominantly to that presumably ocean-generated energy. This biased distribution of amplitudes is part of the reason that noise correlation functions should not typically be interpreted as pure Green's Functions and why we favor the wavefront tracking method (i.e., a method that compares relative measurements along each azimuth).

4. Results

With observations of amplitude variability as wavefronts cross some point in the array, calculated from the right-hand side of equation (1), we can solve for the effect of amplification, attenuation, and internal source terms on the left-hand side. For each location, the observations from both incoming and outgoing wavefields are plotted against the wave propagation azimuth (e.g., Figure 2), and a sine curve with 360° periodicity and some static offset is fit ("1ψ", from *Lin et al.* [2012]). This sine curve describes the direction and magnitude of highest amplification, as well as the overall static loss or addition of energy from attenuation and internal sources, respectively. Note that the observed amplitude variations are generally higher for incoming observations compared to outgoing, which is consistent with the expectation that

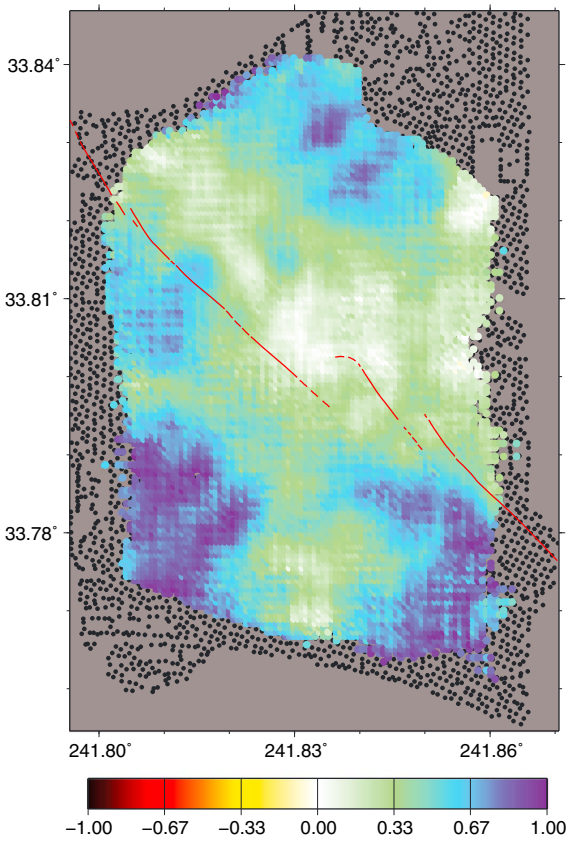

Figure 3. Strength of sources or scattering measured by comparing the incoming and outgoing signals at 0.67 Hz, where enough measurements for both directions are present. Specifically, we subtract the outgoing measurements from the right-hand side of equation (1), for a given azimuth, from the incoming measurements, and average over available azimuths. Incoming signals are sensitive to sources/scatterers, while outgoing signals are not.

internal sources should only add energy to the incoming wavefield. We also note that any elastic effect such as anisotropy should already be removed with the focusing/defocusing term and should not affect our amplitude observations.

While the effect of all three terms on the left-hand side of equation (1) can in theory be distinguished for all locations within the array, in practice we are limited by the inhomogeneous source distribution that is dominated by coastal energy (the northward bias in Figure 1). The incomplete range of azimuthal observations prevents us from confidently determining a 1ψ fit and the spatial pattern of attenuation structure. To quantify the effect of attenuation in general, we estimate the averaged loss of energy across the whole array by averaging all of the amplitude variation measurements of outgoing wavefields, assuming that the directional effects of local amplifications will cancel out. This loss of energy, which we attribute to the intrinsic attenuation term, is 0.22×10^{-3} s km^{-2} averaged for all three frequencies. For comparison, we can consider the averaged difference in static offset between the outgoing and incoming observations where both are available, which relates to the intensity of local sources or scatterers, and these is 0.31×10^{-3} s km^{-2}. Enough observations of both incoming and outgoing measurements are only possible in the center regions of our array, and an example is shown in Figure 3 for our observed source terms at 0.67 Hz. This map correlates with regions of low phase velocity from *Lin et al.* [2013], presented later for reference, which may suggest we are seeing predominantly scattered wavefronts off of damaged material or loose sediments, rather than new sources of impulsive energy. One might have expected to see stronger scattering along strong velocity contrasts, but this is not observed.

Based on the observations above, the attenuation and source terms are relatively small compared to the magnitude of actual variation caused by site amplification. Thus, these small static offsets should not strongly affect the measurement of amplification magnitude and direction, and so we treat the incoming and outgoing signals as approximately equal in order to collect a more complete azimuthal dependence and more robustly fit sine curves. With the directions and magnitudes of maximum amplification for each site, we invert for a single multiplicative factor, β, that best represents site response following the convention of *Lin et al.* [2012]. Maps of β are shown in Figure 4 for 0.67 Hz, 1.0 Hz, and 2.0 Hz, and for comparison, we also show the phase velocity measurements from *Lin et al.* [2013] at the appropriate frequency below each amplification map. The frequencies of the phase velocity maps displayed are different because the depth sensitivity kernels for site amplification and phase velocity vary, and the frequencies are chosen to probe crustal structure of roughly the same depth (see Figure 5). These sensitivity kernels are calculated as in *Lin et al.* [2012], by numerically perturbing shear wave velocities at each depth. We also note that despite site amplification likely having smaller-scale heterogeneity, our final maps have resolution on the order 500 m, which is limited by both station spacing (about 100 m) and the wavelengths involved [*Lin et al.*, 2013].

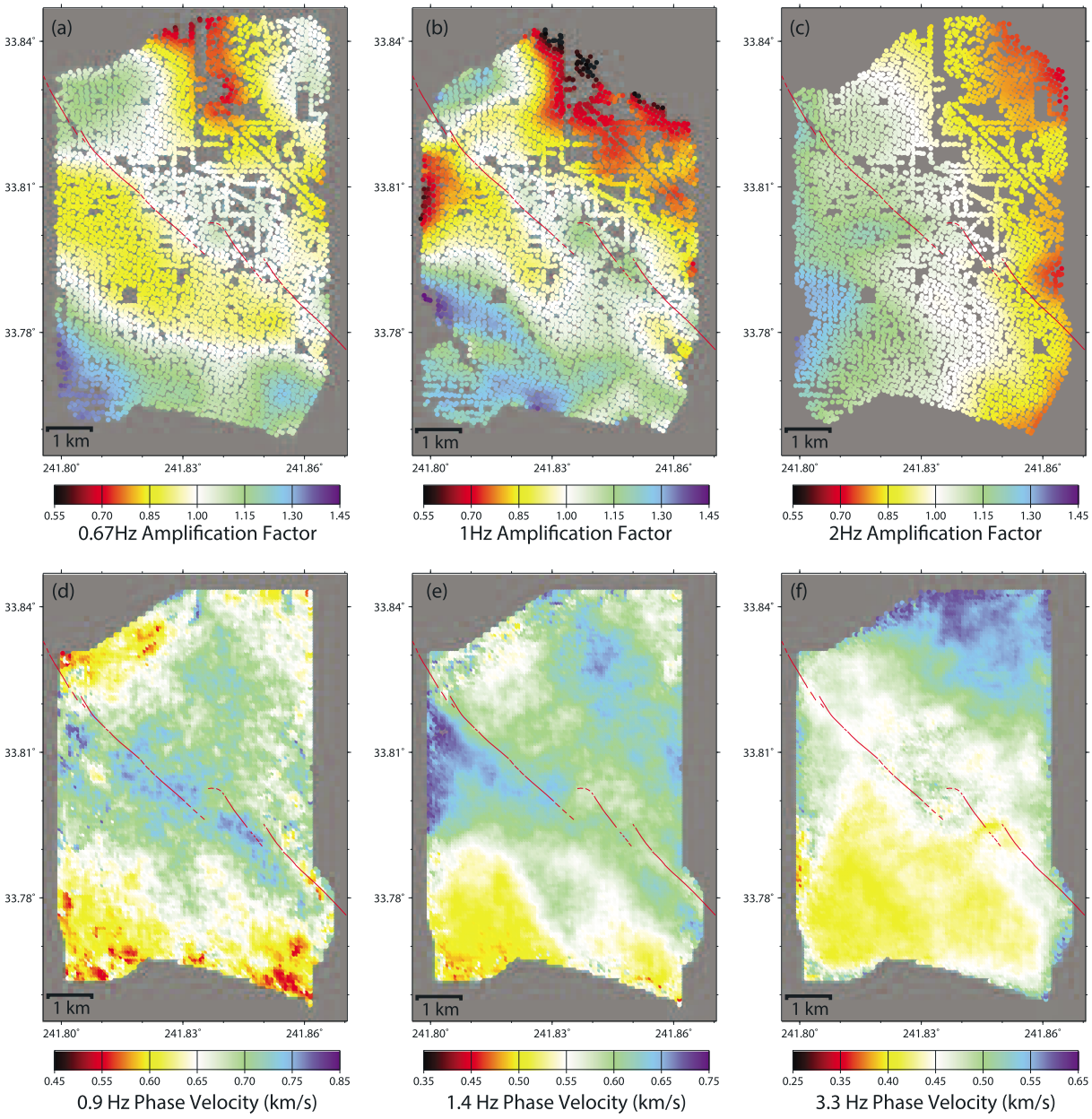

Figure 4. Relative site amplification factors at (a) 0.67 Hz, (b) 1.0 Hz, and (c) 2.0 Hz. Shown below each amplification map is the (d–f) phase velocity map from *Lin et al.* [2013] which has the closest matching sensitivity kernel for the amplification map above it.

These new, high-resolution maps of site amplification show how ground motions are amplified as waves propagate across the array. They suggest that amplitudes in areas to the southwest will be significantly higher than areas to the northeast. These maps also correlate inversely with phase velocities, as might be expected (e.g., decreases in shear wave velocity cause both decreases in phase velocities and increases in amplitude, as shown in Figure 5), but the geometry of the geologic structure and topography act to amplify signals beyond what is prescribed by velocity variations. For example, a sharper contrast of amplitudes across the Newport-Inglewood Fault at 0.67 Hz and 1.0 Hz suggests that the depth and shape of the structure both play a role. Both the 0.67 Hz and 1 Hz maps also show amplification correlating with local topography, notably Signal Hill at the center of the array, where the surface expression of the fault trace is broken. A stronger east-west trend of amplifications observed in the 2.0 Hz map suggest that the short-period, shallow waves are less sensitive to deeper fault structure and instead are more sensitive to surface properties of the sedimentary alluvium, such as compaction, cohesive strength, or water

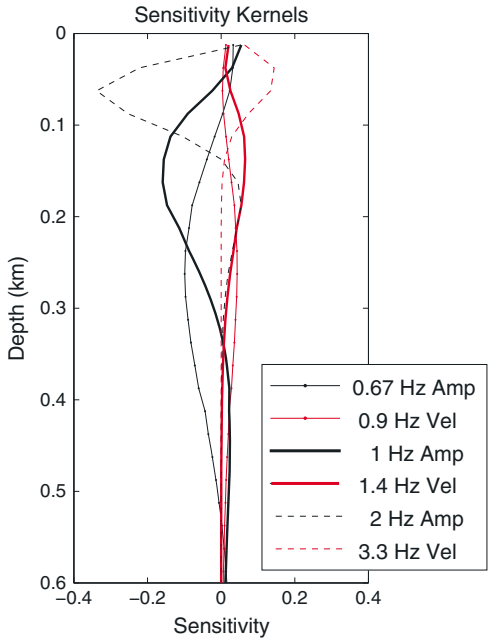

Figure 5. Depth sensitivity kernels for each of the three relative site amplification factors and the three phase velocity maps shown in Figure 4. Note that while the frequencies are different between the site amplification and phase velocity maps compared in Figure 1 (e.g., 1 Hz site amplification and 1.4 Hz phase velocity), they are selected such that they probe similar shear wave velocity structure with depth.

all of which relate to the shear modulus of the material. In fact, because velocity and site amplification are two independent observables, they can potentially also be used to constrain other properties such as density structure [*Lin et al.*, 2012].

Variations in site amplification of this magnitude are expected from earthquake and nuclear testing event observations, such as those by *Rogers et al.* [1979], where peak ground velocity ratios as large as 7 in the Long Beach area are observed. The observed pattern of lower amplifications to the northeast are also observed by *Hauksson et al.* [2008] from the 2008 Chino Hills earthquake. Borehole measurements indicate that our region of low amplifications to the northeast are also characterized by higher clay-silt ratios, thicker Quaternary sediments, and a deeper water table [*Rogers et al.*, 1979]. Modeling by *Saikia et al.* [1994] of seismic data suggest that the variations in sediment thickness act as waveguides which dominate site amplification terms. Also, both observations and theoretical work [e.g., *Sánchez-Sesma and Campillo*, 1991; *Bouchon et al.*, 1996; *Hestholm et al.*, 2006] point out the strong effect of local topography on the amplification and trapping of surface waves. All of these studies illustrate the fact that complex wave propagation interactions are needed to explain observed site amplifications; simple comparisons to velocities or rock types may not be sufficient. High-resolution observations such as provided in this study, which require no assumptions about the structure at depth, are critical for further understanding and modeling of these effects.

5. Conclusions

We have demonstrated that ambient noise tomography can be used to map site amplification at high frequencies in the range 0.67 to 2.0 Hz. Dense arrays, like in Long Beach, CA, open a new opportunity for array processing techniques such as wavefront tracking, but special care is required to preserve relative information across the array. Ambient noise cross correlations in this Long Beach array have a very uneven distribution of noise sources, and their amplitudes would be misinterpreted if used as direct Green's Functions for ground motions. The wavefront tracking approach overcomes this issue by measuring wavefield gradients across the array, regardless of incoming amplitude distributions, and successfully recovers patterns of amplification that are expected from local geology and previous phase velocity observations. Specifically, we find a sharp contrast across the Newport-Inglewood Fault, and generally higher amplitudes to the Southwest of the city. The wavefront tracking approach also yields new information on attenuation and scattering, and offers the potential of spatially resolving these terms if the ambient noise field is omnidirectional enough. These terms are derived from direct observations and are well suited to validate the simulations or modeling which might traditionally be used to estimate such amplifications. Complex interactions of waves moving through the very heterogeneous shallow crust will undoubtedly amplify seismic amplitudes, and direct observations of these effects are the first step toward improving future seismic hazard estimates.

Acknowledgments
The authors gratefully acknowledge Dan Hollis at NodalSeismic LLC, and Signal Hill Petroleum, Inc., for permitting us to use the Long Beach data. We thank Dunzhu Li for scripts and advice in handling the large quantity of cross correlations, and Rob Clayton and Asaf Inbal for helpful discussion. We are also thankful for the constructive and helpful comments from Jesse Lawrence and an anonymous reviewer. This project is supported by NSF grants EAR-1252191, EAR-1214912, and CyberSEES-1442665. Fan-Chi Lin also acknowledges the financial support from Signal Hill Petroleum for this research.

The Editor thanks two anonymous reviewers for their assistance in evaluating this paper.

References

Abrahamson, N. A., and K. M. Shedlock (1997), Overview, *Seismol. Res. Lett.*, *68*(1), 9–23.

Bensen, G. D., M. H. Ritzwoller, M. P. Barmin, A. L. Levshin, F.-C. Lin, M. P. Moschetti, N. M. Shapiro, and Y. Yang (2007), Processing seismic ambient noise data to obtain reliable broad-band surface wave dispersion measurements, *Geophys. J. Int.*, *169*(3), 1239–1260, doi:10.1111/j.1365-246X.2007.03374.x.

Bouchon, M., C. A. Schultz, and M. N. Toksöz (1996), Effect of three-dimensional topography on seismic motion, *J. Geophys. Res.*, *101*(B3), 5835–5846, doi:10.1029/95JB02629.
Cua, G., and T. Heaton (2012), Characterizing average properties of southern California ground motion amplitudes and envelopes, *Bull. Seismol. Soc. Am.*, 1–67.
Denolle, M. A., E. M. Dunham, G. A. Prieto, and G. C. Beroza (2014), Strong ground motion prediction using virtual earthquakes, *Science*, *343*(6169), 399–403, doi:10.1126/science.1245678.
Graves, R., et al. (2010), CyberShake: A physics-based seismic hazard model for Southern California, *Pure Appl. Geophys.*, *168*(3–4), 367–381, doi:10.1007/s00024-010-0161-6.
Hauksson, E., K. Felzer, D. Given, M. Giveon, S. Hough, K. Hutton, H. Kanamori, V. Sevilgen, S. Wei, and A. Yong (2008), Preliminary report on the 29 July 2008 Mw 5.4 Chino Hills, eastern Los Angeles basin, California, earthquake sequence, *Seismol. Res. Lett.*, *79*(6), 855–866.
Hestholm, S., M. Moran, S. Ketcham, T. Anderson, M. Dillen, and G. McMechan (2006), Effects of free-surface topography on moving-seismic-source modeling, *Geophysics*, *71*(6), T159–T166.
Kohler, M. D., P. M. Davis, and E. Safak (2005), Earthquake and ambient vibration monitoring of the steel-frame UCLA factor building, *Earthquake Spectra*, *21*(3), 715–736, doi:10.1193/1.1946707.
Lin, F.-C., M. H. Ritzwoller, and W. Shen (2011), On the reliability of attenuation measurements from ambient noise cross-correlations, *Geophys. Res. Lett.*, *38*, L11303, doi:10.1029/2011GL047366.
Lin, F.-C., V. C. Tsai, and M. H. Ritzwoller (2012), The local amplification of surface waves: A new observable to constrain elastic velocities, density, and anelastic attenuation, *J. Geophys. Res.*, *117*, B06302, doi:10.1029/2012JB009208.
Lin, F.-C., D. Li, R. W. Clayton, and D. Hollis (2013), High-resolution 3D shallow crustal structure in Long Beach, California: Application of ambient noise tomography on a dense seismic array, *Geophysics*, *78*(4), Q45–Q56, doi:10.1190/geo2012-0453.1.
Prieto, G. A., and G. C. Beroza (2008), Earthquake ground motion prediction using the ambient seismic field, *Geophys. Res. Lett.*, *35*, L14304, doi:10.1029/2008GL034428.
Rogers, A. M., J. C. Tinsley, W. W. Hays, and K. W. King (1979), Evaluation of the relation between near-surface geological units and ground response in the vicinity of Long Beach, California, *Bull. Seismol. Soc. Am.*, *69*(5), 1603–1622.
Saikia, C. K., D. S. Dreger, and D. V. Helmberger (1994), Modeling of energy amplification recorded within greater Los Angeles using irregular structure, *Bull. Seismol. Soc. Am.*, *84*(1), 47–61.
Sánchez-Sesma, F. J., and M. Campillo (1991), Diffraction of p, sv, and rayleigh waves by topographic features: A boundary integral formulation, *Bull. Seismol. Soc. Am.*, *81*(6), 2234–2253.
Shapiro, N. M. (2004), Emergence of broadband Rayleigh waves from correlations of the ambient seismic noise, *Geophys. Res. Lett.*, *31*, L07614, doi:10.1029/2004GL019491.
Snieder, R. (2004), Extracting the Green's function from the correlation of coda waves: A derivation based on stationary phase, *Phys. Rev. E: Stat. Nonlinear Soft Matter Phys.*, *69*(4), 046610, doi:10.1103/PhysRevE.69.046610.
Tsai, V. C. (2011), Understanding the amplitudes of noise correlation measurements, *J. Geophys. Res*, *116*, B09311, doi:10.1029/2011JB008483.
Weaver, R. L. (2010), Equipartition and retrieval of Green's function, *Earthquake Sci.*, *23*(5), 397–402, doi:10.1007/s11589-010-0738-2.
Weaver, R. L. (2011), On the retrieval of attenuation from the azimuthally averaged coherency of a diffuse field, *C.R. Geosci.*, *343*, 615–622.
Zhang, J., and X. Yang (2013), Extracting surface wave attenuation from seismic noise using correlation of the coda of correlation, *J. Geophys. Res. Solid Earth*, *118*, 2191–2205, doi:10.1002/jgrb.50186.